Natural marine bromoform emissions in the fully coupled ocean-atmosphere-model NorESM2

Dennis Booge[1,2], Jerry F. Tjiputra[3], Dirk J. L. Olivié[4], Birgit Quack[1] and Kirstin Krüger[2]

[1]GEOMAR Helmholtz Centre for Ocean Research Kiel, Kiel, 241~~48~~05, Germany
[2]Department of Geosciences, Section of Meteorology and Oceanography, University of Oslo, Oslo, 0371, Norway
[3]NORCE Norwegian Research Centre and Bjerknes Centre for Climate Research, Bergen, 5007, Norway
[4]Norwegian Meteorological Institute, Oslo, 0313, Norway

Correspondence to: Dennis Booge (dbooge@geomar.de) and Kirstin Krüger (kkrueger@geo.uio.no)

Abstract. Oceanic bromoform ($CHBr_3$) is an important precursor of atmospheric bromine. Although highly relevant for the future halogen burden and ozone layer in the stratosphere, the global $CHBr_3$ production in the ocean and its emissions are still poorly constrained in observations and are mostly neglected in climate models. Here, we newly implement marine $CHBr_3$ in the state-of-the-art Norwegian Earth System Model (NorESM2) with fully coupled ocean-sea-ice-atmosphere biogeochemistry interactions. Our results are validated with oceanic and atmospheric observations from the HalOcAt (Halocarbons in the Ocean and Atmosphere) data base. The simulated mean oceanic concentrations (6.61±3.43 pmol L^{-1}) are in good agreement with observations in open ocean regions (5.02±4.50 pmol L^{-1}), while the mean atmospheric mixing ratios (0.76±0.39 ppt) are lower than observed but within the range of uncertainty (1.45±1.11 ppt). The NorESM2 ocean emissions of $CHBr_3$ (214 Gg yr^{-1}) are in the range of or higher than previously published estimates from bottom-up approaches but lower than estimates from top-down approaches. Annual mean fluxes are mostly positive (sea-to-air), driven by oceanic concentrations, sea surface temperature and wind speed, dependent on season and location. During winter ~~seasons~~, model results imply some oceanic regions in high latitudes as sinks of atmospheric $CHBr_3$, because of its elevated atmospheric mixing ratios. We further demonstrate that key drivers for the oceanic and atmospheric $CHBr_3$ variability are spatially heterogeneous. In the tropical West Pacific, which is a hot spot for oceanic bromine delivery to the stratosphere, wind speed is the main driver for $CHBr_3$ fluxes on annual basis. In the North Atlantic as well as in the Southern Ocean region the atmospheric and oceanic $CHBr_3$ variabilities are interacting during most of the seasons except for the winter months where sea surface temperature is the main driver. Our study provides improved process understanding of the biogeochemical cycling of $CHBr_3$ and more reliable natural emission estimates especially on seasonal and spatial scales compared to previously published model estimates.

1 Introduction

Bromoform ($CHBr_3$) from the ocean is one of the most important organic compounds for atmospheric bromine with an atmospheric lifetime of ~2-4 weeks (Carpenter and Liss, 2000; Quack and Wallace, 2003; Salawitch, 2006; Papanastasiou et al., 2014). As a reactive halogenated compound, it belongs to the very short-lived substances (VSLS) with lifetimes of less than 6 months in the atmosphere (Law et al., 2007). In the tropics, VSLSs are rapidly lifted to the stratosphere by ~~tropical~~ deep convection (Sala et al., 2014; Navarro et al., 2015; Fuhlbrügge et al., 2016), where they contribute up to ~25% to stratospheric bromine (Dorf et al., 2006 and following work). Bromine is ~60 times more efficient in depleting lower stratospheric ozone than chlorine and significantly contributes to ozone depletion in the lower stratosphere (Daniel et al., 1999; Sinnhuber et al., 2009; Montzka et al., 2011; Villamayor et al., 2023) with potential impacts on the radiation budget of the atmosphere from -0.02 W m^{-2} to -0.13 W m^{-2} (Hossaini et al., 2015; Saiz-Lopez et al., 2023).

The oceanic air-sea gas exchange of $CHBr_3$ is parameterized based on the concentration gradient between surface water and air and is related to wind speed and sea surface temperature via the transfer velocity (e.g., Nightingale et al., 2000).

Due to sparse measurements, marine $CHBr_3$ emission estimates are subject to large uncertainties (Laube et al., 2023). $CHBr_3$ emission inventories from "bottom-up" approaches (e.g., Quack and Wallace, 2003; Butler et al., 2007; Ziska et al., 2013; Lennartz et al., 2015; Stemmler et al., 2015; Fiehn et al., 2018) are based on in-situ oceanic data, whereas "top-down" approaches (e.g., Warwick et al., 2006; Liang et al., 2010; Ordóñez et al., 2012) use in situ atmospheric mixing ratio measurements. Resulting $CHBr_3$ emissions span a large range between 150 and 820 Gg Br yr^{-1} (Laube et al., 2023). The different methods cover e.g., statistical extrapolation of measurement-based data (Ziska et al., 2013; and update in Fiehn et al., 2018), scaling of emissions to chlorophyll-a satellite observations (Ordóñez et al., 2012), modelling atmospheric $CHBr_3$ with a modular flux in a chemistry climate model (Lennartz et al., 2015), and a data-oriented machine-learning algorithm (Wang et al., 2019). These studies use limited spatial and temporal data coverage, underrepresenting seasonal and interannual variations and spatial heterogeneity by averaging concentrations.

Oceanic $CHBr_3$ is mainly linked to primary production through natural processes such as marine organisms like macroalgae and phytoplankton (Gschwend et al., 1985; Carpenter and Liss, 2000; Quack et al., 2004). Elevated surface water concentrations are observed in coastal and shelf waters especially including the eastern boundary upwelling systems (EBUS) (Quack and Wallace, 2003). Laboratory culture studies of phytoplankton production rates by Tokarczyk and Moore (1994) and Moore et al. (1996) reported $CHBr_3$ increase during the exponential growth phase of phytoplankton. Those specific growth rates and the corresponding temporal changes in $CHBr_3$ concentrations were first applied in a physical biogeochemical water column model for the tropical Atlantic (Hense and Quack, 2009), and later implemented in the global biogeochemical HAMburg Ocean Carbon Cycle model (HAMOCC; Stemmler et al., 2015). Stemmler et al. (2015) explicitly implemented sources and sinks of marine $CHBr_3$ in the three-dimensional ocean biogeochemistry model HAMOCC. However, they are not fully coupled with the atmosphere, and resulting fluxes rely on fixed, prescribed, extrapolated, observed atmospheric data of Ziska et al. (2013). Since the atmospheric concentrations are regulated by the oceanic emissions, accurate estimates of atmospheric and oceanic $CHBr_3$ variability require such coupling, which can be achieved using an Earth System Model (ESM).

Here, we present the first global model simulation of $CHBr_3$ in the fully coupled Norwegian ESM (NorESM2), where $CHBr_3$ production is prognostically related to the primary production in the ocean taking natural biological processes into account. We present results from a historical experiment focusing on the period 1990 to 2014 and compare them with HalOcAt observations (https://halocat.geomar.de). Furthermore, we evaluate oceanic $CHBr_3$ excess and deficit regions and use multilinear regression analysis to identify drivers of oceanic and atmospheric $CHBr_3$, as well~~s~~ as $CHBr_3$ emission variations on regional and temporal scales.

2 Model and Methods

We use the latest version of NorESM2 (NorESM2-LM; Seland et al., 2020; Tjiputra et al., 2020), which has participated in the Coupled Model Intercomparison Project phase 6 (CMIP6) and contributed to the latest assessment report of the IPCC-AR6 (Masson-Delmotte et al., 2023). The NorESM2 is a fully coupled ESM and is partly based on the Community ESM Version 2 (Danabasoglu et al., 2020), which is developed by the National Center for Atmospheric Research (NCAR) in the United States. NorESM2 is an updated version of its original version NorESM1 (Bentsen et al., 2013; Tjiputra et al., 2013). It consists of a modified version of the Community Atmosphere Model version 6 (CAM6-Nor), the isopycnic coordinate Bergen Layered Ocean Model (BLOM), the ocean biogeochemistry model isopycnic coordinate HAMOCC (iHAMOCC), the sea ice model (Community Ice CodE version 5.1.2; CICE5.1.2), the Community Land Model version 5 (CLM5), and the river runoff model (MOdel for Scale Adaptive River Transport; MOSART). Both BLOM and iHAMOCC apply a tripolar grid with a horizontal resolution of ~1° and 53 vertical isopycnic layers, while CAM6-Nor and CLM5 share a common horizontal resolution of ~2° and 32 hybrid-pressure layers (lowest atmospheric layer

thickness: ~120 m) and a model top at 3.6 hPa (~40 km altitude). Here, we briefly highlight key features of iHAMOCC as well as the $CHBr_3$ implementation (Section 2.1). The iHAMOCC ocean biogeochemical module is based on the original work of Maier-Reimer (2012), has gone through several improvements and was later adapted to an isopycnic coordinate ocean model (Assmann et al., 2010; Tjiputra et al., 2010). The model prognostically simulates inorganic carbon chemistry following the standard Ocean Model Intercomparison Project (OMIP) protocol. It includes a Nutrient Phytoplankton Zooplankton Detritus (NPZD) type ecosystem module, where the phytoplankton growth rate is constrained by multi-nutrient limitation as well as ambient light and temperature. Particulate organic matters produced in the euphotic zone is exported to the interior with a sinking velocity that increases linearly with depth before it is remineralized back to inorganic carbon. The NorESM2 is able to simulate the observed large-scale pattern of surface primary productivity as well as the regional seasonal cycle (Tjiputra et al., 2020).

2.1 Bromoform module in NorESM2

2.1.1 Oceanic bromoform

The marine $CHBr_3$ processes implemented in iHAMOCC comprise of advection (*adv*), production (β), air-sea gas exchange (*F*), and three sink terms of: photolysis (*UV*), hydrolysis (*H*) and halogen substitution (*S*), as shown in Eq. (1). The production and photolysis occur in the euphotic layer (top 100 m depth) of the model, whereas the air-sea gas exchange is computed in the top-most layer of the ocean (upper 10 m). Advection and other sink terms are calculated throughout the water column. The change over time of the oceanic $CHBr_3$ concentration is modelled as:

$$\frac{[\mathrm{CHBr_3}]}{dt} = adv\text{~~($CHBr_3$)~~} + \beta - F - UV - H - S. \quad (1)$$

The parameterizations for the different processes are largely based on Stemmler et al. (2015). $CHBr_3$ is produced during biological production as follows:

$$\beta = \beta_0 * \left(\frac{f_1 * Si(OH)_4}{K_{phy}^{Si(OH)_4} + Si(OH)_4} + \frac{f_2 * K_{phy}^{Si(OH)_4}}{K_{phy}^{Si(OH)_4} + Si(OH)_4}\right), \quad (2)$$

where $K_{phy}^{Si(OH)_4}$ denotes the half-saturation constant for silicate ($Si(OH)_4$) uptake and diatom and non-diatom contributing factors, f_1 and f_2, are set equally to 1. In contrast to Stemmler et al. (2015), the bulk $CHBr_3$ production ratio (β_0) is modified and set to 2.4×10^{-6} nmol $CHBr_3$ (mmol N)$^{-1}$, based on Kurihara et al. (2012) and Roy (2010).

The air-sea gas exchange is calculated as follows:

$$F = k_w * \left(C_w - \frac{C_a}{H_{bromo}}\right), \quad (3)$$

where C_w and C_a are $CHBr_3$ concentrations in the surface ocean and $CHBr_3$ mixing ratios in the atmosphere, respectively. Emissions are defined as positive fluxes, which means outgassing to the atmosphere, negative fluxes are defined as fluxes from the atmosphere to the ocean . The temperature-dependent dimensionless Henry's law solubility constant (H_{bromo}) is defined in Moore et al. (1995):

$$H_{bromo} = e^{13.16 - \frac{4973}{SST}}, \quad (4)$$

with SST the sea-surface temperature in Kelvin. k_w represents the gas transfer velocity calculated following Nightingale et al. (2000) using the 10 m surface wind speed (u):

$$k_w = (0.222u^2 + 0.33u) * (\frac{660}{Sc_{bromo}})^{0.5}. \quad (5)$$

The Schmidt number (Sc_{bromo}) for $CHBr_3$ is defined in Quack and Wallace (2003) using the sea surface temperature *SST* in °C:

$$Sc_{bromo} = 4662.8 - 319.45 * SST + 9.9012 * SST^2 - 0.1159 * SST^3. \quad (6)$$

The loss term due to photolysis is computed as follows:

$$UV = I_{UV} * \frac{I_0}{I_{ref}} * e^{(-a_w * z)} * [\mathrm{CHBr_3}], \quad (7)$$

where the decay time scale $(I_{UV})^{-1}$ is set to 30 days (Carpenter and Liss, 2000). I_0 and I_{ref} are the prognostic incoming UV radiation (i.e., 30% of shortwave radiation) and annual average irradiance at the surface layer, respectively. z is the depth and a_w is the attenuation coefficient of UV radiation, set to 0.33 m^{-1}.

The loss term related to hydrolysis is estimated following Stemmler et al. (2015):

$$H = A_1 * e^{\left(-\frac{E_A}{RT}\right)} * [\mathrm{OH^-}] * [\mathrm{CHBr_3}], \quad (8)$$

with A_1, E_A, and R set to 1.23x10^{17} L mol^{-1} min^{-1}, 107 300 J mol^{-1}, and 8.314 J K^{-1} mol^{-1}, respectively (Washington, 1995). T is the seawater temperature in Kelvin.

Degradation due to halogen substitution (Eqs. 5-6 of Stemmler et al., 2015):

$$S = L_{ref} * e^{\left(A_2 * (\frac{1}{T_{ref}} - \frac{1}{T})\right)} * [\mathrm{CHBr_3}], \quad (9)$$

with L_{ref} and A_2 set to 7.33x10^{-10} s^{-1} and 12507.13 K, respectively, and T_{ref} = 298 K.

2.1.2 Atmospheric $CHBr_3$

$CHBr_3$ is implemented as a 3-dimensional tracer in the atmospheric model and is transported by the large-scale atmospheric circulation and sub-grid scale processes (shallow and deep convection, and boundary layer turbulence). It is removed in the atmosphere by photolysis:

$$\mathrm{CHBr_3} + hv \rightarrow 3\,Br\,, \quad (10)$$

and by reaction with the OH radical:

$$\mathrm{CHBr_3} + \mathrm{OH} \rightarrow 3\,Br\,. \quad (11)$$

The reaction rate k [cm^3 $molecules^{-1}$ s^{-1}] for the removal of $CHBr_3$ by OH in

$$\frac{d[\mathrm{CHBr_3}]}{dt} = -k * [\mathrm{CHBr_3}] * [\mathrm{OH}] \quad (12)$$

is defined as follows:

$$k = 9.0 * 10^{-13} \exp\left(-\frac{360}{T}\right), \quad (13)$$

with T the ambient temperature in Kelvin, and [$CHBr_3$] and [OH] in molecules cm^{-3}. The loss rate of $CHBr_3$ by photolysis can be expressed by

$$\frac{d[\mathrm{CHBr_3}]}{dt} = -I\ [\mathrm{CHBr_3}], \quad (14)$$

where I [s^{-1}] depends on the intensity of solar radiation and photo-physical properties of $CHBr_3$. The OH concentration is a monthly-varying climatology obtained from a Whole Atmosphere Community Climate Model (WACCM) historical simulation with full tropospheric and stratospheric chemistry (Gettelman et al., 2019).

$CHBr_3$ in the atmosphere has no other sinks than reaction with OH (annual mean $CHBr_3$ lifetime: ~46 days) and photolysis ($CHBr_3$ lifetime: ~23 days) and is not affected by dry or wet deposition.

2.2 Model setup

A historical transient model run from 1850-2014, based on the CMIP6 protocol, was performed following a 500-year preindustrial spin-up. The coupling of $CHBr_3$ between the ocean and the atmosphere is carried out with an hourly time frequency exchanging the air-sea gas transfer. For analysis of the model climatology as well as for analysis of the model validation with observations and further analysis of the driving $CHBr_3$ factors, daily model output data was averaged over a period of 25 years (1990-2014) resulting in one mean value for each day of the year. The standard deviation of each day reflects the variability within this time period. The 1990 to 2014 interval was chosen as most of the observations for the model validation are within that time period, as compiled in the HalOcAt database (https://halocat.geomar.de, last access: 13.10.2023).

2.3 Observations: HalOcAt database

The HalOcAt database, compiled by Ziska et al. (2013), updated by Fiehn et al. (2018) and by this study, is an observation-based database for global oceanic and atmospheric data of short-lived halogenated compounds, such as $CHBr_3$. To date, there are 9369 oceanic and 65179 atmospheric $CHBr_3$ measurements listed in 68 oceanic and 156 atmospheric datasets (campaigns), respectively. The following criteria were applied to the observations in order to be used for model validation:

- Sampling locations with an ocean bottom depth less than 200 m or closer than 100 km to land were excluded.
- Sampling depth of oceanic $CHBr_3$ measurements had to be within the first 10 m of the water column in order to be comparable to the $CHBr_3$ output of the upper surface ocean model layer (10 m depth).
- Maximum sampling height of atmospheric $CHBr_3$ measurements was set to 30 m altitude.
- Wherever applicable, individual measurements throughout one day were averaged to result in a daily averaged surface ocean concentration or atmospheric mixing ratio in order to consider the same temporal resolution as the daily model output. The coordinates of the respective averaged data points throughout a day were also equally averaged. These locations were used to compare the observation with the closest grid point of the model output.

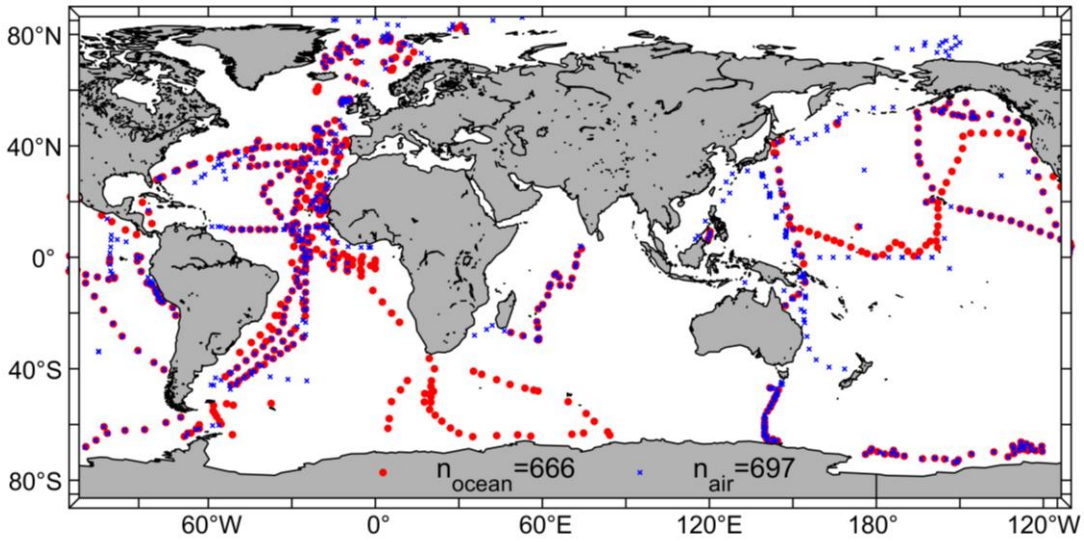

Figure 1: Locations of oceanic (red, n=666) and atmospheric (blue, n=697) daily mean $CHBr_3$ observations from the HalOcAt database used to compare to daily mean NorESM2 model output.

After screening the HalOcAt data base with the above-mentioned criteria, the individual oceanic and atmospheric datasets (including the remaining datapoints) were tested for outliers. The mean from each dataset was calculated and the group of all average values was tested for outliers. An outlier was defined as an element with more than three standard deviations from the mean. According to the outlier test for oceanic and atmospheric datasets the corresponding dataset was removed and not used for further validation of the model.

By addressing the mentioned criteria and datasets, we were able to validate the model with 666 daily mean oceanic (5154 individual) and 697 daily mean atmospheric (8411 individual) $CHBr_3$ observations from the HalOcAt database covering both hemispheres (northern hemisphere (NH): 61%, southern hemisphere (SH): 39%), from the tropics (0-20°N/°S; 36%) to the polar regions (60-90°N/S; 18%) with most observations in or above the Atlantic Ocean (44%) (Figure 1).

2.4 Bromoform excess/deficit calculation

The $CHBr_3$ excess/deficit (balance) rate (k_{bal}, Eq. (15), pmol m^{-2} h^{-1}) is the difference between the $CHBr_3$ production rate and the sum of different $CHBr_3$ loss rates, with all rates integrated over the upper 100 m depth):

$$k_{bal} = \sum production\ rate - \sum loss\ rate = k_{\beta} - (k_{UV} + k_F). \quad (15)$$

The production term is described as the biological oceanic $CHBr_3$ production rate (k_{β}, Eq. (2)) and the loss term includes the two fastest loss processes, i.e., photolysis due to UV radiation (k_{UV}, Eq. (7)) and the loss to the atmosphere via air-sea gas exchange (k_F, Eq. (3)). We define a positive k_{bal} as $CHBr_3$ excess rate and a negative k_{bal} as $CHBr_3$ deficit rate. The loss terms related to hydrolysis and to halogen substitution are not included as they are several orders of magnitude smaller than k_{UV} and k_F, in the surface ocean.

2.5 Calculation of drivers for oceanic and atmospheric $CHBr_3$ and its emissions

Different parameters impact the variations of oceanic and atmospheric $CHBr_3$ values and influence the air-sea gas exchange. These impacts can vary in magnitude and frequency dependent on local and seasonal conditions. Daily mean average model output values from 1990-2014 were used to calculate annual and seasonally resolved (DJF, MAM, JJA, SON) driving factors for oceanic $CHBr_3$ concentrations ($Bromo_{oce}$), atmospheric $CHBr_3$ mixing ratios ($Bromo_{air}$) and $CHBr_3$ fluxes ($Bromo_{flux}$) in three different specific areas (North Atlantic, tropical West Pacific, Southern Ocean), which

are presented in Section 3.4. Driving factors for each area, parameter and season were derived using multilinear regression (MLR) analyses.

In order to compare parameters with different magnitudes, input data of each parameter was standardized prior to MLR analysis by centering to have a mean of 0 and scaled to have a standard deviation of 1. Input data for each parameter consisted of daily mean averages over the specific area, providing 365 values as basis for annually and ~ 90 values for seasonally resolved MLR.

A schematic summarizing the relationships between the different parameters in Eqs. (S1-S3) is shown in Fig. 2 including $CHBr_3$ production ($Bromo_{prod}$), the 10 m surface wind speed (*wind*), the sea surface temperature (*SST*) and the derived parameters $Bromo_{oce}$, $Bromo_{air}$ and $Bromo_{flux}$. Other oceanic $CHBr_3$ loss processes (e.g., photolysis) were neglected in these calculations as the loss due to gas exchange is ~70 times higher than the loss due to photolysis (data not shown). If the highest resulting coefficient for each season and MLR is significantly higher than all other coefficients, the corresponding parameter is presented as the main driver for either $Bromo_{oce}$, $Bromo_{air}$ or $Bromo_{flux}$. If the highest resulting coefficient is not significantly different from the second or third highest coefficient, more than one coefficient and corresponding parameters are presented as main drivers. Table 1 lists the annual mean coefficients, Table S1 lists the seasonally resolved main drivers.

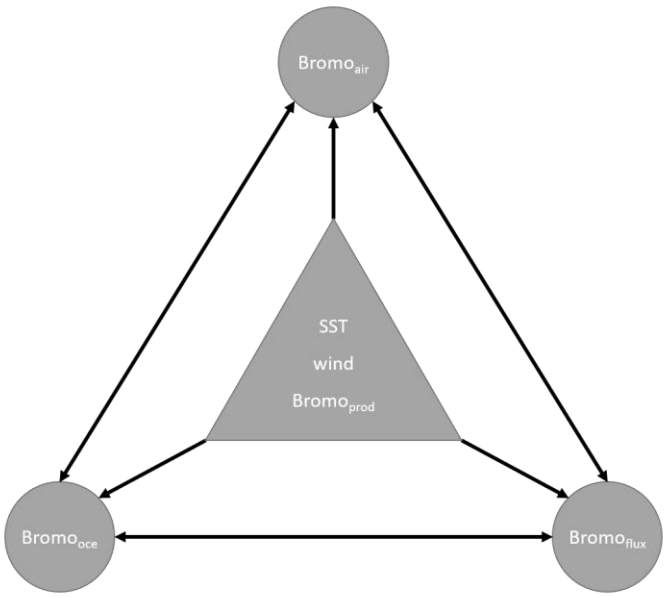

Figure 2: Schematic illustration of relationships between different parameters influencing each other. Generic parameters in triangle influence the derived parameters in circles. Each derived parameter in a circle is influenced by all other five parameters. Relationships are the basis for the multilinear regression analysis using Eqs. (S1-S3).

3 Results and Discussion

3.1 Model climatology

The annual and seasonal $CHBr_3$ oceanic concentrations, atmospheric mixing ratios and emissions reveal significant spatial variations (Figure 3, S1). The annual global average surface $CHBr_3$ concentrations are 5.04 pmol L^{-1} (DJF: 5.36 pmol L^{-1}, JJA: 4.86 pmol L^{-1}) with highest annual mean concentrations of 28.37 pmol L^{-1} in the upwelling region off the coast of Peru and lowest annual mean concentrations of 1.37 pmol L^{-1} in the Gulf of Boothia (71°N, 91°W) north of Canada. The areas with the lowest oceanic $CHBr_3$ concentrations are the central parts of the North and the South Pacific Gyres. Concentrations of surface ocean $CHBr_3$ in the entire NH (JJA: 5.9 pmol L^{-1} > DJF: 4.3 pmol L^{-1}) and SH (DJF: 6.1 pmol L^{-1} > JJA: 4.1 pmol L^{-1}) are generally higher during the respective summer than during the respective winter ~~season~~. These distinct differences of oceanic $CHBr_3$ concentrations are also due to the higher biological production in summer (NH: 335 pmol m^{-2} h^{-1}; SH: 371 pmol m^{-2} h^{-1}) than in winter (NH: 235 pmol m^{-2} h^{-1}; SH: 173 pmol m^{-2} h^{-1}) as shown in Fig. S3 and discussed in Section 3.4. The direct link of $CHBr_3$ to the biological production applies to the low oceanic $CHBr_3$ concentrations in the North and South Pacific Gyres and to the high oceanic concentrations in the areas of the EBUS.

Variations in annual mean atmospheric $CHBr_3$ mixing ratios mainly follow the surface ocean concentrations with highest mixing ratios in the tropics, especially in the EBUS. Global annual average mixing ratios over the ocean are 0.67 ppt (DJF: 0.70 ppt, JJA: 0.69 ppt) with highest annual mean mixing ratios of 2.21 ppt in the south-eastern Pacific upwelling region off the coast of Peru and lowest annual mean mixing ratios of 0.13 ppt over the Persian Gulf. On a global average, the variability of atmospheric mixing ratios is lower than the variability of $CHBr_3$ concentrations in the surface ocean (Figure 3, S2). During austral winter (JJA), mostly dark and cold conditions increase the lifetime of atmospheric $CHBr_3$, which leads to a uniform mixing ratio (0.67±0.05 ppt) over the entire Southern Ocean. Similar to oceanic $CHBr_3$ concentrations, central parts of the North and South Pacific Gyre have low atmospheric $CHBr_3$ mixing ratios (0.46±0.05 ppt). During austral summer (DJF) atmospheric mixing ratios increase further as strong biological activity increases surface ocean concentrations, which enhance the oceanic emissions. Further seasonal dependent driving factors for specific regions are discussed in Section 3.4.

Generally, supersaturation of $CHBr_3$ in the world's ocean leads to emissions from the ocean to the atmosphere (defined as positive fluxes). Global annual mean fluxes are 268 pmol m^{-2} h^{-1} (DJF: 294 pmol m^{-2} h^{-1}, JJA: 253 pmol m^{-2} h^{-1}) with highest annual mean fluxes of 953 pmol m^{-2} h^{-1} in the upwelling region off the coast of Peru. In the tropical regions, annual mean fluxes of 427 pmol m^{-2} h^{-1} between 10°N and 10°S, add to atmospheric entrainment of oceanic $CHBr_3$ up into the stratosphere (Fiehn et al., 2018; Tegtmeier et al., 2020). Lowest annual mean fluxes of -1 pmol m^{-2} h^{-1} are modelled under ice free conditions in the Gulf of Boothia (71°N, 91°W) north of Canada (white regions in Figure 3) with very low oceanic $CHBr_3$ production and low seawater temperatures. However, the atmospheric mixing ratios are comparably high under these conditions. These conditions favour negative fluxes, which, according to the results of our fully coupled ESM, can be seen in the Arctic and Antarctic during winter ~~season~~, confirming the results by Stemmler et al. (2015) and Ziska et al. (2013) although with a lower magnitude.

Generally, the modelled $CHBr_3$ emissions are high, where the ocean concentration is high and the elevated emissions lead to elevated atmospheric mixing ratios. However, due to oceanic transport processes, locations of high oceanic $CHBr_3$ emissions do not always coincide with locations of high oceanic $CHBr_3$ production (compare Figure 3 and Fig. S3). In the northern part of the Bay of Bengal (>18°N) e.g., ocean concentrations during DJF are very high (average: 21.64 pmol L^{-1}), while the emissions are not as high compared to other ocean regions, due to low wind speeds. This leads to a lower atmospheric mixing ratio than expected from the oceanic concentrations and shows that oceanic $CHBr_3$ concentrations and emissions as well as atmospheric mixing ratios show regionally different interdependencies, which is addressed in detail in Section 3.4.

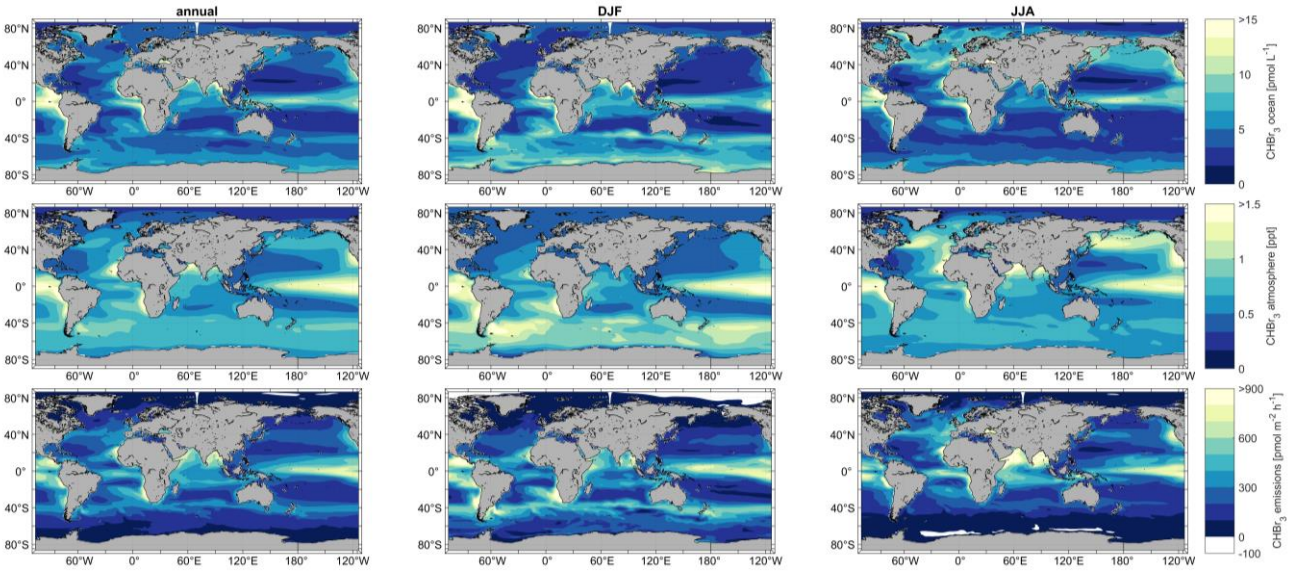

Figure 3: Simulated annual (left), DJF (middle) and JJA (right) mean oceanic surface $CHBr_3$ concentrations (upper panel), atmospheric mixing ratios (middle panel) and $CHBr_3$ emissions (lower panel) for the period 1990-2014.

3.2 Model validation with observations

The annual mean surface oceanic $CHBr_3$ concentration (Figure 4a) from the 666 daily mean observations is $5.02^{28.21}_{0.05}$ ($mean^{max}_{min}$) pmol L^{-1} ~~with a 25th and 75th percentile of 2.19 and 6.16 pmol L^{-1}, respectively (min: 0.05 pmol L^{-1}, max: 28.21 pmol L^{-1}, mean: 5.02 pmol L^{-1})~~. The global annual mean surface oceanic $CHBr_3$ concentration from the model using only locations corresponding with an existing observation is $6.61^{24.25}_{1.39}$ pmol L^{-1} ~~with a 25th and 75th percentile of 4.23 and 8.10 pmol L^{-1}, respectively (min: 1.39 pmol L^{-1}, max: 24.25 pmol L^{-1}, mean: 6.61 pmol L^{-1})~~. These results indicate that the model values are in the range with observed concentrations of oceanic $CHBr_3$. While the mean concentration of the model is higher than the mean of the observations, all validated model data points fall within the full range of the observations. The model data cover a grid of ~100 km resolution, which leads to a smoothing of the values, whereas observational data is local daily mean point data.

The mean $CHBr_3$ atmospheric mixing ratio (Figure 4b) from the 697 daily mean observations is $1.45^{9.80}_{0.03}$ ppt ~~with a 25th and 75th percentile of 0.78 and 1.71 ppt, respectively (min: 0.03 ppt, max: 9.80 ppt)~~. The global mean atmospheric mixing ratio of $CHBr_3$ from the model at locations with observations is $0.76^{2.70}_{0.22}$ ppt ~~with a 25th and 75th percentile of 0.49 and 0.90 ppt, respectively (min: 0.22 ppt, max: 2.70 ppt)~~. This comparison shows that the observed atmospheric mixing ratios of $CHBr_3$ are in the same magnitude but generally higher than those from the model output. While our model experiment focuses on natural $CHBr_3$ production by phytoplankton, other sources as coastal macroalgae (Carpenter and Liss, 2000) and anthropogenic sources, such as power plant cooling (Maas et al., 2021) or desalination plants (Agus et al., 2009), may explain parts of the higher global annual median observational data of 41%. Jia et al. (2023) calculated an increase

of global $CHBr_3$ emissions of 31.5% when including anthropogenic emissions, which partly can also explain the lower observed atmospheric mixing ratios in the model compared to the observations.

Figure 4 also shows a more detailed comparison between observations and model data in 5° meridional binned averages (shaded areas) for oceanic (Figure 4c) and atmospheric (Figure 4d) $CHBr_3$ on annual basis as well as in JJA and DJF. The modelled data compare well with observations of oceanic $CHBr_3$ (Figure 4c) on annual basis over the 5° latitudinal bins. In the HalOcAt database, there are no oceanic and atmospheric observations available north of 50°N and south of 30°S during boreal (DJF) and austral winter (JJA), respectively, which highlights the need of model data to entirely describe spatially and temporally resolved $CHBr_3$ (see also Fiehn et al., 2018). During DJF, the model overestimates the

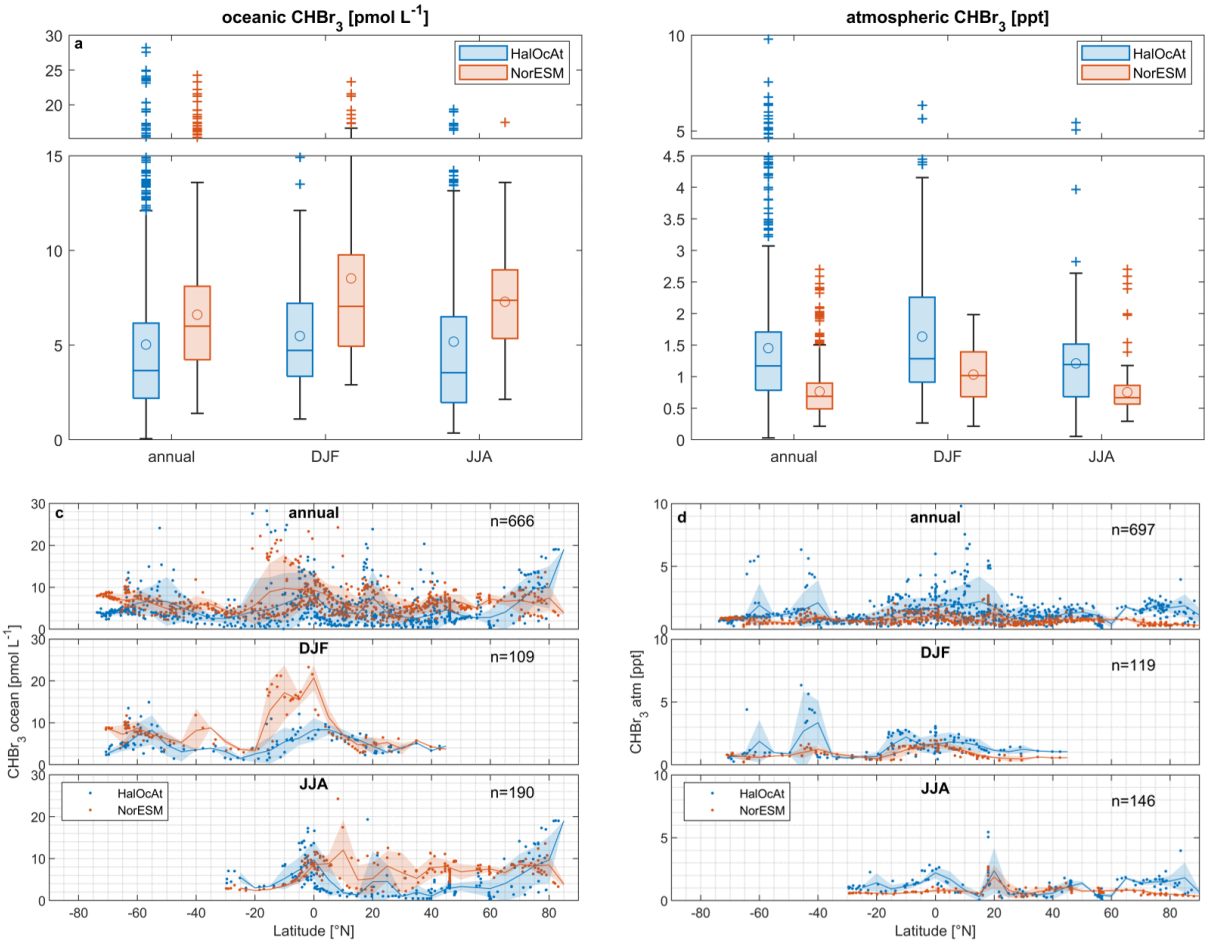

Figure 4: Boxplot comparison of NorESM2 model results with HalOcAt observations for oceanic (a) and atmospheric $CHBr_3$ (b), c: zonal mean oceanic $CHBr_3$ comparison annually and in DJF and JJA, d: zonal mean atmospheric $CHBr_3$ comparison annually and in DJF and JJA. Shaded areas are standard deviations from 5° zonal bin averages. Boxplots (left) have a break in the y axis to increase readability of the figure. The line inside the box represents the median value, the circle the mean value, the boxes show the first to third quartile, and the whiskers illustrate the highest and lowest values that are not outliers. The plus signs represent outliers.

measured concentrations between 20°N and 5°S. During JJA, averaged model concentrations in the NH (10°N – 60°N) are slightly higher than the averaged observations. These discrepancies could indicate a missing process understanding, revealing lower oceanic production or additional loss processes.

With all data available, the 5° latitudinal averaged atmospheric $CHBr_3$ observations have a large spread in the tropics resulting in a high standard deviation (Figure 4d). The model results in this region are uniform with a much lower standard deviation. During boreal winter (DJF) atmospheric $CHBr_3$ observations and model results show a good agreement, with an exception at 40-50°S. In this latitude range, observational atmospheric $CHBr_3$ mixing ratios (>3 ppt, Figure 4d) were recorded between 24° and 60° W in the South Atlantic in 2007 (Gebhardt, 2008). Gebhardt (2008) reports enhanced biological production in the Argentinian shelf-break zone (55°-60° W) with elevated chlorophyll-*a* concentration up to 4.5 µg L^{-1}. These values suggest also a high production of $CHBr_3$ and subsequent high emissions to the atmosphere. The

prevailing westerly winds, transported the $CHBr_3$ enriched air masses eastward to the remote South Atlantic region in 2007, while in the model lower biological production entails lower atmospheric mixing ratios compared to the observations. During boreal summer (JJA) very good agreement between atmospheric observations and model results is obtained between 10°N and 60°N. North of 60°N, the model underestimates the measured atmospheric mixing ratios in the polar region. Local meteorological and biological conditions (e.g., high wind speed, distinct phytoplankton blooms) are averaged by the model to a resolution of ~100 km. Averaging data over time or space leads to lower mean values (i.e., gas emissions, Bates and Merlivat, 2001) in the model. ~~, which~~This explains lower modelled atmospheric mixing ratios compared to the observations on a global scale~~. These local and short-term temporal variations contribute to the discrepancy in atmospheric values at global scale as well as potential~~ together with anthropogenic $CHBr_3$ ~~emissions~~ sources (Jia et al., 2023). Furthermore, discrepancies between model results and observations also point to missing process understanding, which helps to improve our understanding of the biogeochemical cycling of $CHBr_3$. For our $CHBr_3$ production rate, we used the highest production rate, which we could retrieve from the published data (Roy, 2010; Kurihara et al., 2012). Therefore, we likely do not underestimate the oceanic planktonic source in general, and either the production rates are too high or the sink rates are too low in some regions, e.g., the equatorial Pacific. Furthermore, the resulting model bias does not follow a spatial pattern (Fig. S4). We claim, that currently not enough observational or experimental information is available to narrow down on the answer. As pointed out, the underestimation of atmospheric $CHBr_3$, despite the maximum of the planktonic $CHBr_3$ source is likely due to averaging, a missing source for the atmosphere or even the parameterization of marine $CHBr_3$ fluxes yielding too low emission values. Despite the named uncertainties, which deserve further studies, the model reflects very well the data and therewith the current status of knowledge.

3.3 Excess and deficit regions of oceanic bromoform

In most of the world's surface oceans (e.g., North and South Pacific) $CHBr_3$ production and loss rates are balanced on an annual average with a k_{bal} close to zero (top panel of Figure 5). The equator region experiences a strong excess rate (positive k_{bal}) on annual average with values up to 300 pmol m^{-2} h^{-1} showing higher $CHBr_3$ production than loss of $CHBr_3$ in the upper ocean, caused by strong primary production (Fig. S3) in the equatorial upwelling. Surface currents transport the $CHBr_3$ enriched surface water masses away from the equator, while experiencing loss of $CHBr_3$ to the atmosphere. Therefore, adjacent marine areas north and south of the equator experience a deficit rate (negative k_{bal}) of $CHBr_3$ (blue areas, Figure 5), as no production balances the loss. The seasonality of k_{bal} is pronounced in the extratropics (bottom panels of Figure 5). In these regions, a $CHBr_3$ excess rate is observed mainly during summer and a $CHBr_3$ deficit rate mainly during winter in the respective hemispheres. A high k_β (elevated biological production) and a low k_F (weak emissions to the atmosphere) caused by lower winds during summer, lead to a higher $CHBr_3$ surface ocean concentration in summer compared to winter time (Figure 3). During winter in both hemispheres, lower biological activity (low k_β) and elevated wind speed (high k_F) decrease the $CHBr_3$ production and increase the emissions to the atmosphere, which leads to a $CHBr_3$ deficit rate. These results reveal seasonal as well as spatial differences in parameters (driving factors), which influence $CHBr_3$ concentrations in the world's ocean.

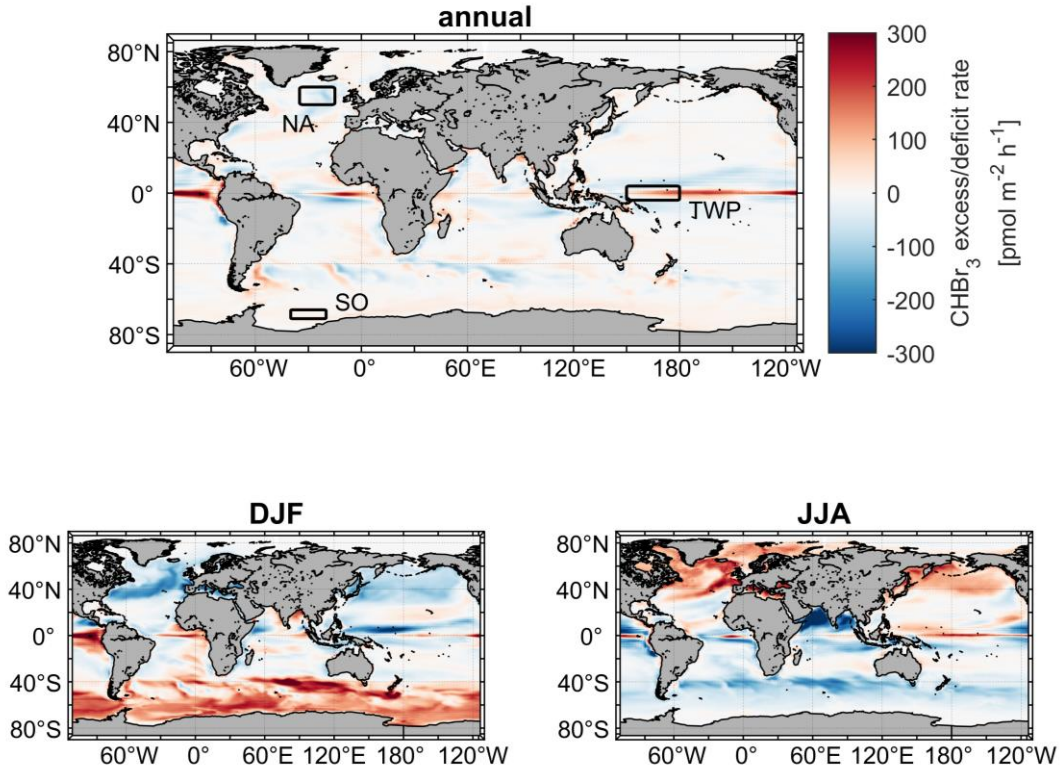

Figure 5: Mean $CHBr_3$ excess/deficit rates on annual (top) and seasonal (DJF: bottom left; JJA: bottom right) basis. Three rectangles in the top figure illustrate locations of case studies. NA: North Atlantic; TWP: Tropical West Pacific; SO: Southern Ocean.

In the following subsection, we selected three different case study areas, indicated in Figure 5, in order to contrast the driving factors of the variations of oceanic and atmospheric $CHBr_3$ on regional and temporal scales:

- North Atlantic, with an annual mean $CHBr_3$ deficit rate (k_{bal} = -33 pmol m^{-2} h^{-1})
- Tropical West Pacific, with an annual mean $CHBr_3$ excess rate (k_{bal} = +32 pmol m^{-2} h^{-1})
- Southern Ocean, with negative fluxes during the respective winter ~~season~~ (k_{bal} = +15 pmol m^{-2} h^{-1})

3.4 Driving factors of bromoform on regional and temporal scales

This section investigates the seasonal changes of oceanic and atmospheric $CHBr_3$ and other parameters in three contrasting regions. Daily means of oceanic $CHBr_3$ concentrations, production, fluxes, balance (as defined in Eq. (15)), atmospheric mixing ratios as well as SST and wind speed, over an entire year reveal large differences between the North Atlantic, tropical West Pacific, and Southern Ocean (Figure 6). With MLR analysis, the main driving factors of oceanic and atmospheric $CHBr_3$ variability and its fluxes in each region and season are investigated.

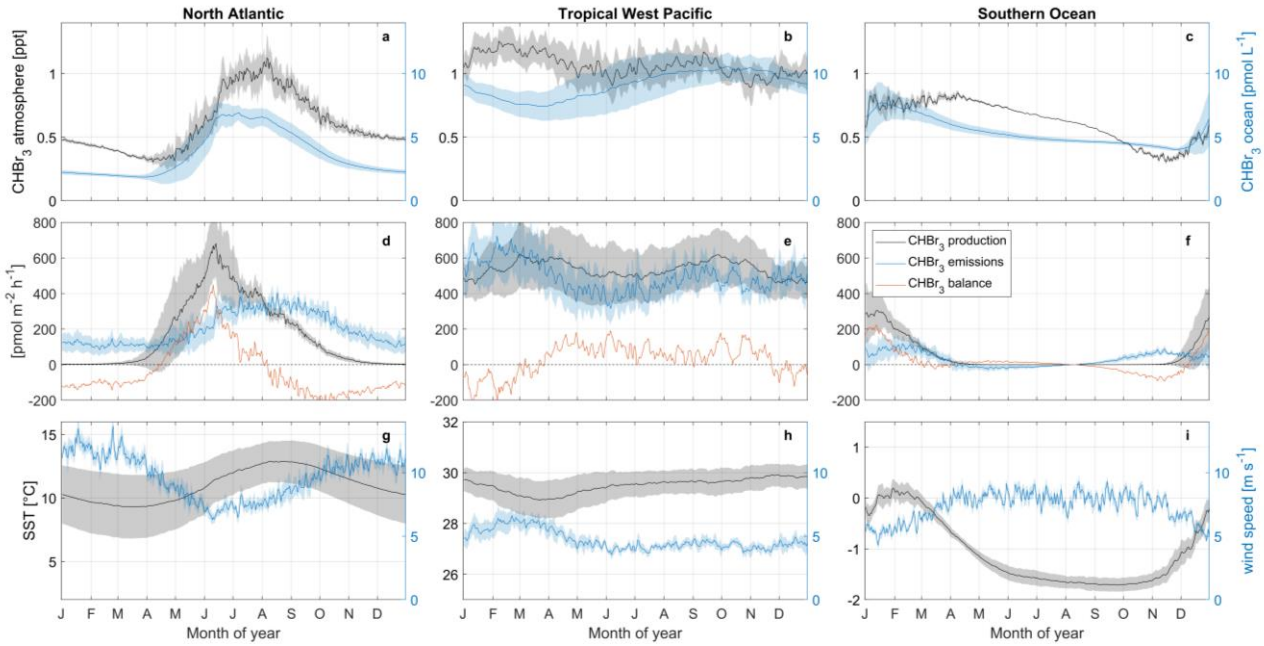

Figure 6: Seasonal changes of oceanic and atmospheric $CHBr_3$ (upper panel, a-c), $CHBr_3$ production, emissions and balance (middle panel, d-f), SST and wind speed (bottom panel, g-i), in the North Atlantic (left), tropical west Pacific (middle) and Southern Ocean (right). Shaded area is one standard deviation of the average value in the corresponding area. Note: y-limits for SST are not similar in between the three regions in order to increase readability of the figure.

North Atlantic

The North Atlantic region (50°N – 60°N, 15°W – 35°W) is characterized by a strong seasonal cycle of both oceanic $CHBr_3$ concentrations and atmospheric mixing ratios (Figure 6a). The magnitude of the cycle is strongest among the three investigated regions (compare with Figure 6b,c). Oceanic $CHBr_3$ concentrations are on average 3.64 pmol L^{-1} (min:1.87 pmol L^{-1} during end of March; max: 6.93 pmol L^{-1} during July). Atmospheric mixing ratios show a similar seasonal cycle, shifted by one month, with average values of 0.60 ppt, a minimum mixing ratio of 0.30 ppt during April and a maximum mixing ratio of 1.12 ppt during August. The $CHBr_3$ emissions (199±91 pmol m^{-2} h^{-1}) follow the pattern of both oceanic and atmospheric values (Figure 6d). The seasonal cycle of $CHBr_3$ production (171±191 pmol m^{-2} h^{-1}) is similar to the cycle of $CHBr_3$ concentration, while the sharp peak in May/June when the spring phytoplankton bloom evolves in the North Atlantic, is not reflected in the oceanic concentrations. The strong production leads to a $CHBr_3$ excess rate during summer (JJA: 103 pmol m^{-2} h^{-1}) and a $CHBr_3$ deficit rate in winter time (DJF: -114 pmol m^{-2} h^{-1}), respectively (Figure 6d).

The MLR analysis indicates, that on an annual basis, variations in atmospheric mixing ratios are mainly associated with CHBr3 ocean concentrations (Table 1, ~~R^2=0.89, p-value<0.05~~) and vice versa (Figure 7a,d). A higher surface water CHBr3 concentration increases the emissions to the atmosphere resulting in increasing atmospheric mixing ratios. According to the MLR analysis on a seasonal basis, oceanic CHBr3 concentrations are mainly driven by the oceanic production during MAM ~~(R^2=0.93, p-value<0.05)~~ and SON ~~(R^2=0.99, p-value<0.05)~~ (Table S1), which increases from March to June sharply to 680 pmol m-2 h-1 before gradually decreasing in SON (Figure 6d). Atmospheric mixing ratios are mainly driven by the oceanic concentration (Figure 7d, Table 1, R^2=0.89, p-value<0.05). Only in winter (DJF), where hardly any production occurs, low SSTs, which increase the solubility of $CHBr_3$ drive the atmospheric mixing ratio variations (Table S1, R^2=0.95, p-value<0.05). Thus, the emissions decrease, even during high wind speeds, which leads to lower atmospheric $CHBr_3$. The emissions are mainly driven by the oceanic concentrations (Figure 7g, Table 1, R^2=0.81, p-value<0.05) over the course of a year, while during spring (MAM) wind speed, SST, and $CHBr_3$ production drive the

emissions equally (Table S1). While $CHBr_3$ production and SSTs increase, surface wind speed decreases and emissions are pretty constant at 130±29 pmol m^{-2} h^{-1} (Figure 6d). During summer (JJA), low winds and a high oceanic $CHBr_3$ concentration equally increase the emissions (Table S1). In contrast to spring, higher SSTs (lower solubility) are only of minor importance during JJA, while in autumn and winter the decreasing SSTs are the main drivers again together with high atmospheric mixing ratios, which additionally dampen the emissions (Table S1).

Tropical West Pacific

Figure 5 shows that the equatorial regions of the Atlantic and Pacific Oceans are a source of oceanic $CHBr_3$, which is transported to other oceanic regions by ocean currents. $CHBr_3$ ocean concentrations in the tropical West Pacific (4°S – 4°N, 150°E – 180°E) show a reduced seasonal cycle in comparison to the above discussed North Atlantic region (Figure 6b), while the average of 9.11 pmol L^{-1} is significantly higher than in the North Atlantic. Also, $CHBr_3$ production (536±42 pmol m^{-2} h^{-1}), $CHBr_3$ fluxes (492±84 pmol m^{-2} h^{-1}) and atmospheric mixing ratios (1.07±0.08 ppt) show hardly any seasonality (Figure 6b, e). The same is true for SST (29.50±0.28 °C) and wind speed (4.71±0.76 m s^{-1}) (Figure 6h). The $CHBr_3$ balance is positive throughout the whole year except for DJF (Figure 6e). During this period high wind speed entails higher emission. Production rates are lower and induce a $CHBr_3$ deficit. However, this deficit does not compensate for the $CHBr_3$ excess during the rest of the year leading to an overall excess of 32 pmol m^{-2} h^{-1}.
MLR analysis shows that the wind speed is the main factor influencing the variations of oceanic $CHBr_3$ concentrations ~~(R^2=0.51, p-value<0.05)~~, $CHBr_3$ atmospheric mixing ratios ~~(R^2=0.74, p-value<0.05)~~, and $CHBr_3$ fluxes ~~(R^2=0.73, p-value<0.05)~~ on an annual basis (Figure 7b,e,h, Table 1). During JJA and SON $CHBr_3$ production drives the $CHBr_3$ concentrations (Table S1~~, JJA: R^2=0.43, p-value<0.05, SON: R^2=0.51, p-value<0.05~~) which increases from 477 pmol m^{-2} h^{-1} in July to 618 pmol m^{-2} h^{-1} by the end of September. This results in an increase of oceanic $CHBr_3$ concentrations as all other parameters stay constant during that period.

Southern Ocean

The selected Southern Ocean region (71°S – 66°S, 40°W – 20°W) experiences generally negative water temperatures (mean: -1.08°C) around the year (Figure 6i). The minimum of -1.71°C is reached in September and the maximum of +0.19°C in January/February. Wind speed is nearly constant throughout the year (7.33 m s^{-1}) decreasing only during austral summer (DJF, Figure 6h) to 5.76 m s^{-1} . Oceanic $CHBr_3$ concentrations are on average higher (5.38 pmol L^{-1}) than in the North Atlantic region. Maximum concentrations of 7.74 pmol L^{-1} are reached in January and lowest concentrations of 4.04 pmol L^{-1} end of December. Due to low SSTs as well as a short daylength, $CHBr_3$ production rates are almost zero from May to October and increase to 306 pmol m^{-2} h^{-1} in January (Figure 6f). Atmospheric mixing ratios are highest (0.85 ppt) from January to beginning of April and decline very slowly (Figure 6c) under the following low light levels until they reach their minimum of 0.31 ppt in November. Constant high atmospheric mixing ratios, very low SST, and decreasing oceanic $CHBr_3$ concentrations after the short summer bloom in DJF, influence the switch from emissions~~positive~~ to negative fluxes between April and July (Figure 6f). $CHBr_3$ is in excess during times of production (DJF), almost balanced during the autumn and wintertime from April to September (Figure 6f), with a slight excess of 15 pmol m^{-2} h^{-1} annually.

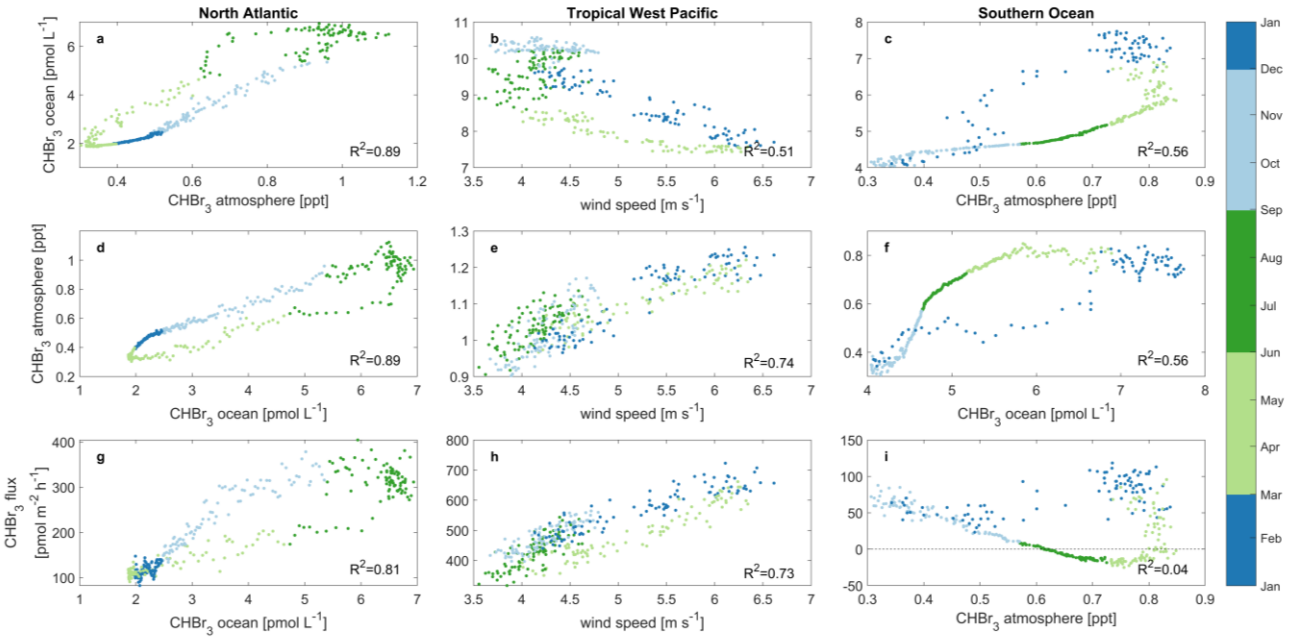

Figure 7: Main drivers of oceanic $CHBr_3$ concentrations (a, b, c), atmospheric mixing ratios (d, e, f) and $CHBr_3$ emissions (g, h, i) in the North Atlantic (a, d, g), tropical West Pacific (b, e, h) and Southern Ocean (c, f, i). Different colours denote different seasons of the year. Each data point represents a daily mean average over the specific case study area. Statistical analysis for each of the nine datasets indicates significant correlation (p-value<0.05) with coefficient of determination (R^2) listed in bottom right of each sublot. Please be aware that subplots a and d as well as c and f contain the same information only with interchanged x and y axes, as both parameters, oceanic and atmospheric bromoform, are interdependent in the two regions.

Atmospheric mixing ratios are the main factor influencing the variations of oceanic concentrations (Figure 7c, Table 1, R^2=0.56, p-value<0.05), while during autumn (MAM, Table S1) $CHBr_3$ production is its driving factor. During this time $CHBr_3$ production decreases and so does the ocean concentration (Figure 6c,f). The atmospheric mixing ratio is mainly driven by high oceanic $CHBr_3$ concentrations in DJF: R^2=0.88, p-value<0.05 and by SST during the cold JJA: R^2=0.95, p-value<0.05) (Table S1). Low light levels increase the lifetime of atmospheric $CHBr_3$ in JJA and the low SSTs increase the solubility of oceanic $CHBr_3$, both leading to decreased ~~sea-to-air~~ emissions during winter (JJA). $CHBr_3$ emissions are mainly driven by SST in summer (DJF) (Table S1, R^2=0.60, p-value<0.05), as the solubility of $CHBr_3$ in the ocean decreases due to the increasing SSTs. After this short summer period, temperatures decline in autumn (MAM) and increase the solubility of oceanic $CHBr_3$, which results in decreased emissions (Figure 6f,i). During winter (JJA) and spring (SON), SSTs and oceanic $CHBr_3$ concentrations stay low and therefore, increasing emissions are mainly driven by decreasing atmospheric mixing ratios.

In summary, the three different regions clearly indicate that driving factors for atmospheric and oceanic bromoform as well as for bromoform fluxes are dependent on local conditions. Planktonic production, which is the only source for $CHBr_3$ in the model set-up impacts the variability of oceanic $CHBr_3$ concentrations only in regions with a distinct seasonality (i.e., North Atlantic, Southern Ocean) in biological production. During times of lower productivity, atmospheric mixing ratios influence the oceanic $CHBr_3$ concentration. In subpolar and polar regions (i.e., Southern Ocean), oceanic $CHBr_3$ and its subsequent fluxes are driven by its solubility related to the low SST in late winter and spring (i.e., sea-ice melt). Although wind speed is an important parameter for the air-sea gas flux, this study reveals that wind speed is only the main driver for oceanic and atmospheric $CHBr_3$ variability in areas with low seasonality (i.e., Tropical West Pacific).

These results demonstrate the benefits of simulating $CHBr_3$ in a fully coupled ESM configuration to calculate driving factors for different parameters on temporal and spatial basis. Studying the influence of one or more parameters on the variability of other parameters in the model is not realistic when using prescribed oceanic concentrations or atmospheric

mixing ratios. Investigating the $CHBr_3$ cycling in different locations and different time scales helps to understand their interconnection and to better integrate their results in today's as well as in a future climate.

Table 1: Annual coefficients of predictors for each MLR in the different case studies. Bold coefficients are the highest value within a MLR analysis of one parameter and region and act as indicator for the driving factors of the predicted parameter (Eqs. S1-S3).

	Predictor parameter	North Atlantic	Tropical West Pacific	Southern Ocean
$CHBr_3$ ocean concentration	Wind speed	-0.02	**-0.96**	-0.10
	SST	<0.01	<0.01	<0.01
	Atm. mixing ratio	**0.68**	0.19	**0.60**
	$CHBr_3$ production	0.39	0.13	0.53
	$CHBr_3$ fluxes	<0.01	<0.01	<0.01
$CHBr_3$ atmospheric mixing ratio	Wind speed	0.29	**0.94**	0.55
	SST	0.32	<0.01	<0.01
	Ocean concentration	**0.93**	0.12	**1.07**
	$CHBr_3$ production	<0.01	0.02	<0.01
	$CHBr_3$ fluxes	<0.01	<0.01	<0.01
$CHBr_3$ fluxes	Wind speed	0.20	**1.27**	0.21
	SST	0.67	0.50	0.53
	Ocean concentration	**0.83**	0.16	1.00
	$CHBr_3$ production	<0.01	0.10	<0.01
	Atm. mixing ratio	-0.32	-0.02	**-1.22**

3.5 Global bromoform emission inventories

A comparison of our modelled versus published global $CHBr_3$ emissions are presented in Figure 8. Global annual $CHBr_3$ emissions from top-down approaches are 449 Gg yr^{-1}, 528 Gg yr^{-1} and 592 Gg yr^{-1} based on calculations from Liang et al. (2010), Ordóñez et al. (2012) and Warwick et al. (2006), respectively. These inventories are about two to eight times higher than calculated annual emissions from bottom-up approaches, which are in the range of 76 Gg yr^{-1} (Stemmler et al., 2015) to 238 Gg yr^{-1} (Lennartz et al., 2015). Our results (214 Gg yr^{-1}) are similar to emission estimates published by Ziska et al. (2013) of 215 Gg yr^{-1} but significantly higher than the 76 Gg yr^{-1} estimate by Stemmler et al. (2015), which is based on the oceanic $CHBr_3$ observations from HalOcAt.

As we apply a 2.38 higher $CHBr_3$ production rate in the ocean as Stemmler et al. (2015), we simulate a production rate of 0.88 Gmol yr^{-1} compared to 0.37 Gmol yr^{-1} by Stemmler et al. (2015). Our emissions (214 Gg yr^{-1}) are 2.82 times higher (Figure 8, global values) compared to the emission estimate (76 Gg yr^{-1}) from Stemmler et al. (2015). Our model

adaption is based on the higher bulk $CHBr_3$ production ratio (β_0) according to Kurihara et al. (2012) and Roy (2010) (see Section 2.1.1). This production rate is at the higher end of published values. Therefore, the resulting $CHBr_3$ production can be seen as an upper limit. Moreover, the ratio of bromoform emissions (ratio: 2.82) is higher compared to the ratio of bromoform production (ratio: 2.38) and indicates an excess of 18%. This is caused by the prescribed mean atmospheric values without any seasonality used in Stemmler et al. (2015) and gets more significant with higher latitudes where seasonality of bromoform emissions becomes more important (Fiehn et al., 2018). Especially during winter times annually mean prescribed atmospheric values are too high and artificially dampen the bromoform emissions. This results in a higher emission estimate using our fully coupled model approach.

Comparing bottom-up and top-down approaches, the annual $CHBr_3$ emissions from the tropics (20°S – 20°N, Figure 8) account for ~47% (105 Gg yr^{-1}) and ~66% (351 Gg yr^{-1}) of global emissions, respectively. The tropics only account for ~37% of global oceanic surface though, underlining this region as the most important source region of $CHBr_3$ of the earth. Emissions in the middle latitudes (20 to 50°N/S) of the NH and SH show a similar distinction between top-down and bottom-up approaches. However, the annual $CHBr_3$ emissions are only half that of the tropics. Natural open ocean emission estimates from our study are proportional to the surface area between NH and SH in the middle latitudes. This relationship is reversed for the top-down approach estimates. Top-down emission estimates are higher in the NH compared to the SH although the oceanic surface area is lower in the NH (17%) compared to the SH (26%). This indicates the strong influence of coastal emissions on observational atmospheric mixing ratios used in top-down approaches.

In the high latitudes (50-90°N/S), emissions of bottom-up approaches are in the same range (SH) and even higher (NH) compared to top-down approaches (Figure 8). In the northern polar region (8% of global oceanic surface area), $CHBr_3$ emissions from our study account for 3% (6 Gg yr^{-1}) of global emissions and are significantly lower than the other two bottom-up approaches from Lennartz et al. (2015) (11%, 27 Gg yr^{-1}) and Ziska et al. (2013) (21%, 45 Gg yr^{-1}), which appears mainly due to the resolved seasonality within our study. According to the HalOcAt database, no measurements are recorded from November to February and from May to September north of 50°N in the NH and south of 50°S in the SH, respectively. Therefore, the prescribed atmospheric values in Ziska et al. (2013) and in Stemmler et al. (2015) are biased to the ice-free summer months, with higher atmospheric mixing ratios, thus artificially dampening the ~~emissions from the ocean to the atmosphere during~~ winter emissions ~~seasons~~. Due to the influence of the annually fixed prescribed atmospheric mixing ratios in Stemmler et al. (2015), negative fluxes are more pronounced between 50°N/S and 70°N/S up to -100 pmol m^{-2} h^{-1} at ~ 60°N/S. Our lesser negative fluxes in the coupled ESM approach appear more realistic as they are not based on summer biased prescribed values.

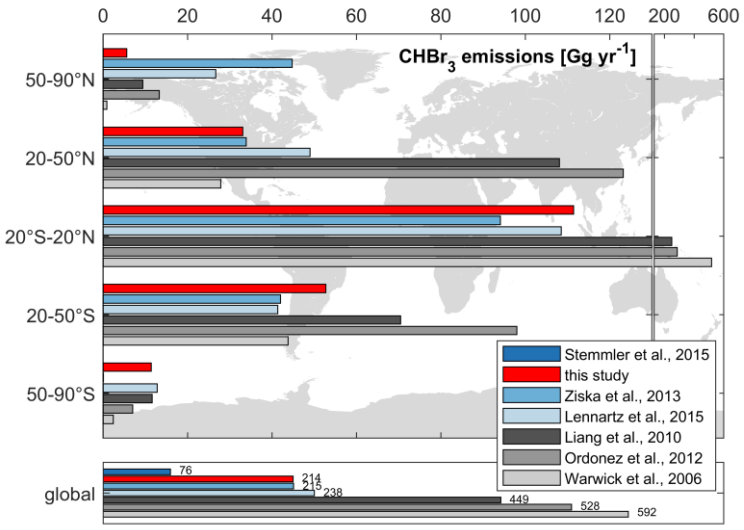

Figure 8: Comparison of global and latitudinally binned annual $CHBr_3$ emissions from different studies. Grey and blue bars denote top-down and bottom-up approaches, respectively.

Our global $CHBr_3$ emission inventory indicates distinct differences to the top-down approaches reflecting only 40%-50% of global emissions calculated by Liang et al. (2010), Ordóñez et al. (2012) and Warwick et al. (2006). Atmospheric $CHBr_3$ values in the top-down approaches are higher than the calculated atmospheric mixing ratios from our fully coupled

model analysis. Those~~They~~ include elevated coastal sources (Scenario A and C, Liang et al., 2010), which may partly explain the discrepancy.

An additional explanation for the overall higher atmospheric mixing ratios of $CHBr_3$ from observations could be that observations from coastal areas (100 km within the coastline) were excluded from this study and are not represented in the model, as they are difficult to quantify (i.e., tide-dependent $CHBr_3$ emissions of macroalgae) with a horizontal model resolution of 1°. However, coastal emissions lead to higher atmospheric mixing ratios of $CHBr_3$ (Fuhlbrügge et al., 2013; Fuhlbrügge et al., 2016; Hepach et al., 2016), which can be transported to remote open ocean regions, while these higher observational values are not included in the model results (Figure 4).

Another explanation for the underestimation of the modelled atmospheric mixing ratios compared to observations is the use of air-sea gas exchange parameterizations, whose uncertainty is estimated to be 25% (Wanninkhof, 2007) and may be underestimated up to 75% (Yang et al., 2022) at low wind speeds.

4 Conclusions and Outlook

Our study is the first one to derive oceanic and atmospheric $CHBr_3$ concentrations, as well as fluxes, from a fully coupled ESM simulation. The model prognostically simulates oceanic $CHBr_3$ production by phytoplankton and includes oceanic $CHBr_3$ loss due to air-sea gas exchange, photolysis, hydrolysis and halogen substitution. Atmospheric loss of $CHBr_3$ is described by photolysis and the reaction with OH. We validate the model results with more than 5,100 oceanic and 8,400 atmospheric observations from the HalOcAt database. The simulated global mean $CHBr_3$ emission rate (214 Gg yr^{-1}) is in the range of previously published bottom-up approaches (76-238 Gg yr^{-1}), but significantly lower than top-down approaches (449-592 Gg yr^{-1}). The model allows to realistically resolve seasonal and spatial variations and to identify different drivers of oceanic and atmospheric $CHBr_3$ variability on regional and seasonal scales. Our results indicate that only during high productive seasons a consequently high $CHBr_3$ production drives high oceanic $CHBr_3$ concentrations. During low productive seasons, relatively high atmospheric mixing ratios suppress the gas exchange and consequently influence variations in oceanic $CHBr_3$ concentrations. In tropical regions (e.g., tropical West Pacific) with a small seasonal cycle, but high oceanic concentrations and atmospheric mixing ratios, wind speed is the main factor driving the variability of oceanic and atmospheric $CHBr_3$ and its fluxes. The results clearly indicate the benefit of a fully coupled ocean-atmosphere-biogeochemistry ESM. In earlier modelling studies, prescribed, fixed atmospheric or oceanic values were applied, which bias the seasonal impact of different factors on oceanic and atmospheric $CHBr_3$ and subsequently induce additional uncertainties to the magnitude of $CHBr_3$ emissions.

Our fully coupled ocean atmosphere approach resolves natural biogenic oceanic and atmospheric $CHBr_3$ including their fluxes at relatively high temporal and spatial model resolution. Validation with observational data shows good agreement for large scale spatial patterns and we attribute the remaining model-data differences to missing coastal, both natural and anthropogenic, sources, which are not implemented in the model. Comparison with other published $CHBr_3$ inventories indicates that approaches without seasonality lack to resolve $CHBr_3$ fluxes especially in high latitudes.

Our results demonstrate the potential for applying a fully coupled ESM to elucidate the primary drivers of the observed $CHBr_3$ concentrations and fluxes variability across spatial and temporal scales. Moreover, this model set-up allows to implement additional oceanic derived VSLS in order to further investigate their influence on the atmospheric chemistry. The dissociation of open ocean natural derived $CHBr_3$ from coastal area derived $CHBr_3$ in this study reveal that coastal derived $CHBr_3$ influences open ocean atmospheric mixing ratios. Therefore, implementing natural coastal next to anthropogenic sources and concurrent model resolution increase in these areas will help to further close the gap of published $CHBr_3$ emission estimates between bottom-up and top-down approaches. Long-term future changes in $CHBr_3$ dynamics under various scenarios should be investigated with a fully coupled ESM, to study the impact of climate change

on $CHBr_3$ dynamics, i.a., in the Arctic, associated with loss of sea-ice and its climate feedback through interaction with ozone chemistry.

Data availability. Observational data can be made accessible by contacting the principal investigator of HalOcAt through https://halocat.geomar.de. Model data will be archived and will be made available upon request.

Author contributions.

DB wrote the manuscript and led the discussion with contributions from all authors. DB analysed the model simulations and prepared the graphics. JFT and DJLO implemented the $CHBr_3$ model code changes in NorESM2 in discussion with BQ and all other authors. JFT carried out the model runs. KK led this project and initiated the research idea for this study.

Competing interests. The authors declare that they have no conflict of interest.

Acknowledgements. This work was financed by the Research Council of Norway through the KeyCLIM project (295046) within the KLIMAFORSK/POLARFORSK program. Resources for the model simulations and data storage were provided by Sigma2 - the National Infrastructure for High Performance Computing and Data Storage in Norway.

References

Agus, E., Voutchkov, N., and Sedlak, D. L.: Disinfection by-products and their potential impact on the quality of water produced by desalination systems: A literature review, Desalination, 237, 214-237, 10.1016/j.desal.2007.11.059, 2009.

Assmann, K. M., Bentsen, M., Segschneider, J., and Heinze, C.: An isopycnic ocean carbon cycle model, Geoscientific Model Development, 3, 143-167, DOI 10.5194/gmd-3-143-2010, 2010.

Bates, N. R. and Merlivat, L.: The influence of short-term wind variability on air-sea CO exchange, Geophysical Research Letters, 28, 3281-3284, Doi 10.1029/2001gl012897, 2001.

Butler, J. H., King, D. B., Lobert, J. M., Montzka, S. A., Yvon-Lewis, S. A., Hall, B. D., Warwick, N. J., Mondeel, D. J., Aydin, M., and Elkins, J. W.: Oceanic distributions and emissions of short-lived halocarbons, Global Biogeochemical Cycles, 21, Artn Gb1023 10.1029/2006gb002732, 2007.

Carpenter, L. J. and Liss, P. S.: On temperate sources of bromoform and other reactive organic bromine gases, Journal of Geophysical Research-Atmospheres, 105, 20539-20547, Doi 10.1029/2000jd900242, 2000.

Danabasoglu, G., Lamarque, J. F., Bacmeister, J., Bailey, D. A., DuVivier, A. K., Edwards, J., Emmons, L. K., Fasullo, J., Garcia, R., Gettelman, A., Hannay, C., Holland, M. M., Large, W. G., Lauritzen, P. H., Lawrence, D. M., Lenaerts, J. T. M., Lindsay, K., Lipscomb, W. H., Mills, M. J., Neale, R., Oleson, K. W., Otto-Bliesner, B., Phillips, A. S., Sacks, W., Tilmes, S., van Kampenhout, L., Vertenstein, M., Bertini, A., Dennis, J., Deser, C., Fischer, C., Fox-Kemper, B., Kay, J. E., Kinnison, D., Kushner, P. J., Larson, V. E., Long, M. C., Mickelson, S., Moore, J. K., Nienhouse, E., Polvani, L., Rasch, P. J., and Strand, W. G.: The Community Earth System Model Version 2 (CESM2), Journal of Advances in Modeling Earth Systems, 12, e2019MS001916, ARTN e2019MS001916 10.1029/2019MS001916, 2020.

Daniel, J. S., Solomon, S., Portmann, R. W., and Garcia, R. R.: Stratospheric ozone destruction: The importance of bromine relative to chlorine, Journal of Geophysical Research-Atmospheres, 104, 23871-23880, Doi 10.1029/1999jd900381, 1999.

Dorf, M., Butler, J. H., Butz, A., Camy-Peyret, C., Chipperfield, M. P., Kritten, L., Montzka, S. A., Simmes, B., Weidner, F., and Pfeilsticker, K.: Long-term observations of stratospheric bromine reveal slow down in growth, Geophysical Research Letters, 33, Artn L24803 10.1029/2006gl027714, 2006.

Fiehn, A., Quack, B., Stemmler, I., Ziska, F., and Krüger, K.: Importance of seasonally resolved oceanic emissions for bromoform delivery from the tropical Indian Ocean and west Pacific to the stratosphere, Atmospheric Chemistry and Physics, 18, 11973-11990, 10.5194/acp-18-11973-2018, 2018.

Fuhlbrügge, S., Krüger, K., Quack, B., Atlas, E., Hepach, H., and Ziska, F.: Impact of the marine atmospheric boundary layer conditions on VSLS abundances in the eastern tropical and subtropical North Atlantic Ocean, Atmospheric Chemistry and Physics, 13, 6345-6357, 10.5194/acp-13-6345-2013, 2013.

Fuhlbrügge, S., Quack, B., Tegtmeier, S., Atlas, E., Hepach, H., Shi, Q., Raimund, S., and Krüger, K.: The contribution of oceanic halocarbons to marine and free tropospheric air over the tropical West Pacific, Atmospheric Chemistry and Physics, 16, 7569-7585, 10.5194/acp-16-7569-2016, 2016.

Gebhardt, S.: Biogenic emission of halocarbons, Mainz, Univ., Diss., 2008, 10.25358/openscience-2211, 2008.

Gettelman, A., Mills, M. J., Kinnison, D. E., Garcia, R. R., Smith, A. K., Marsh, D. R., Tilmes, S., Vitt, F., Bardeen, C. G., McInerny, J., Liu, H. L., Solomon, S. C., Polvani, L. M., Emmons, L. K., Lamarque, J. F., Richter, J. H., Glanville, A. S., Bacmeister, J. T., Phillips, A. S., Neale, R. B., Simpson, I. R., DuVivier, A. K., Hodzic, A., and Randel, W. J.: The Whole Atmosphere Community Climate Model Version 6 (WACCM6), Journal of Geophysical Research-Atmospheres, 124, 12380-12403, 10.1029/2019jd030943, 2019.

Gschwend, P. M., Macfarlane, J. K., and Newman, K. A.: Volatile halogenated organic compounds released to seawater from temperate marine macroalgae, Science, 227, 1033-1035, 10.1126/science.227.4690.1033, 1985.

Hense, I. and Quack, B.: Modelling the vertical distribution of bromoform in the upper water column of the tropical Atlantic Ocean, Biogeosciences, 6, 535-544, DOI 10.5194/bg-6-535-2009, 2009.

Hepach, H., Quack, B., Tegtmeier, S., Engel, A., Bracher, A., Fuhlbrügge, S., Galgani, L., Atlas, E. L., Lampel, J., Friess, U., and Krüger, K.: Biogenic halocarbons from the Peruvian upwelling region as tropospheric halogen source, Atmospheric Chemistry and Physics, 16, 12219-12237, 10.5194/acp-16-12219-2016, 2016.

Hossaini, R., Chipperfield, M. P., Montzka, S. A., Rap, A., Dhomse, S., and Feng, W.: Efficiency of short-lived halogens at influencing climate through depletion of stratospheric ozone, Nature Geoscience, 8, 186-190, 10.1038/Ngeo2363, 2015.

Jia, Y., Hahn, J., Quack, B., Jones, E., Brehon, M., and Tegtmeier, S.: Anthropogenic Bromoform at the Extratropical Tropopause, Geophysical Research Letters, 50, e2023GL102894, ARTN e2023GL102894 10.1029/2023GL102894, 2023.

Kurihara, M., Iseda, M., Ioriya, T., Horimoto, N., Kanda, J., Ishimaru, T., Yamaguchi, Y., and Hashimoto, S.: Brominated methane compounds and isoprene in surface seawater of Sagami Bay: Concentrations, fluxes, and relationships with phytoplankton assemblages, Marine Chemistry, 134, 71-79, 10.1016/j.marchem.2012.04.001, 2012.

Laube, J. C., Tegtmeier, S., Fernandez, R. P., Harrison, J., Hu, L., Krummel, P., Mahieu, E., Park, S., and Western, L.: Update on Ozone-Depleting Substances (ODSs) and Other Gases of Interest to the Montreal Protocol, 978-9914-733-97-6, 2023.

Law, K., Sturges, W., Blake, D., Blake, N., Burkholder, J., Butler, J., Cox, R., Haynes, P., Ko, M., and Kreher, K.: Halogenated very short-lived substances, Chapter 2 in: Scientific Assessment of Ozone Depletion: 2006, Global Ozone Research and Monitoring Project–Report No. 50, World Meteorological Organization, Geneva, Switzerland, 572, 2007.

Lennartz, S. T., Krysztofiak, G., Marandino, C. A., Sinnhuber, B. M., Tegtmeier, S., Ziska, F., Hossaini, R., Krüger, K., Montzka, S. A., Atlas, E., Oram, D. E., Keber, T., Bönisch, H., and Quack, B.: Modelling marine emissions and atmospheric distributions of halocarbons and dimethyl sulfide: the influence of prescribed water concentration vs. prescribed emissions, Atmospheric Chemistry and Physics, 15, 11753-11772, 10.5194/acp-15-11753-2015, 2015.

Liang, Q., Stolarski, R. S., Kawa, S. R., Nielsen, J. E., Douglass, A. R., Rodriguez, J. M., Blake, D. R., Atlas, E. L., and Ott, L. E.: Finding the missing stratospheric Br: a global modeling study of CHBr3 and CH2Br2, Atmospheric Chemistry and Physics, 10, 2269-2286, DOI 10.5194/acp-10-2269-2010, 2010.

Maas, J., Tegtmeier, S., Jia, Y., Quack, B., Durgadoo, J. V., and Biastoch, A.: Simulations of anthropogenic bromoform indicate high emissions at the coast of East Asia, Atmospheric Chemistry and Physics, 21, 4103-4121, 10.5194/acp-21-4103-2021, 2021.

Maier-Reimer, E.: Geochemical cycles in an ocean general circulation model. Preindustrial tracer distributions, Global Biogeochemical Cycles, 7, 645-677, 10.1029/93gb01355, 2012.

Masson-Delmotte, V., Zhai, P., Pirani, A., Connors, S. L., Péan, C., Berger, S., Caud, N., Chen, Y., Goldfarb, L., Gomis, M. I., Huang, M., Leitzell, K., Lonnoy, E., Matthews, J. B. R., Maycock, T. K., Waterfield, T., Yelekçi, O., Yu, R., Zhou, B., and Ipcc: Annex I: Observational Products, in: Climate Change 2021 – The Physical Science Basis, Cambridge University Press, Cambridge, United Kingdom and New York, NY, USA, 2061-2086, 10.1017/9781009157896.015, 2023.

Montzka, S. A., Reimann, S., Engel, A., Kruger, K., Sturges, W. T., Blake, D., Dorf, M., Fraser, P., Froidevaux, L., and Jucks, K.: Ozone-depleting substances (ODSs) and related chemicals (chapter 1), 2011.

Moore, R. M., Geen, C. E., and Tait, V. K.: Determination of Henry's Law constants for a suite of naturally occurring halogenated methanes in seawater, Chemosphere, 30, 1183-1191, 10.1016/0045-6535(95)00009-w, 1995.

Moore, R. M., Webb, M., Tokarczyk, R., and Wever, R.: Bromoperoxidase and iodoperoxidase enzymes and production of halogenated methanes in marine diatom cultures, Journal of Geophysical Research-Oceans, 101, 20899-20908, Doi 10.1029/96jc01248, 1996.

Navarro, M. A., Atlas, E. L., Saiz-Lopez, A., Rodriguez-Lloveras, X., Kinnison, D. E., Lamarque, J. F., Tilmes, S., Filus, M., Harris, N. R., Meneguz, E., Ashfold, M. J., Manning, A. J., Cuevas, C. A., Schauffler, S. M., and Donets, V.: Airborne measurements of organic bromine compounds in the Pacific tropical tropopause layer, Proc Natl Acad Sci U S A, 112, 13789-13793, 10.1073/pnas.1511463112, 2015.

Nightingale, P. D., Malin, G., Law, C. S., Watson, A. J., Liss, P. S., Liddicoat, M. I., Boutin, J., and Upstill-Goddard, R. C.: In situ evaluation of air-sea gas exchange parameterizations using novel conservative and volatile tracers, Global Biogeochemical Cycles, 14, 373-387, Doi 10.1029/1999gb900091, 2000.

Ordóñez, C., Lamarque, J. F., Tilmes, S., Kinnison, D. E., Atlas, E. L., Blake, D. R., Sousa Santos, G., Brasseur, G., and Saiz-Lopez, A.: Bromine and iodine chemistry in a global chemistry-climate model: description and evaluation of very short-lived oceanic sources, Atmospheric Chemistry and Physics, 12, 1423-1447, 10.5194/acp-12-1423-2012, 2012.

Papanastasiou, D. K., McKeen, S. A., and Burkholder, J. B.: The very short-lived ozone depleting substance CHBr (bromoform): revised UV absorption spectrum, atmospheric lifetime and ozone depletion potential, Atmospheric Chemistry and Physics, 14, 3017-3025, 10.5194/acp-14-3017-2014, 2014.

Quack, B. and Wallace, D. W. R.: Air-sea flux of bromoform: Controls, rates, and implications, Global Biogeochemical Cycles, 17, 10.1029/2002gb001890, 2003.

Quack, B., Atlas, E., Petrick, G., Stroud, V., Schauffler, S., and Wallace, D. W. R.: Oceanic bromoform sources for the tropical atmosphere, Geophysical Research Letters, 31, Artn L23s05 10.1029/2004gl020597, 2004.

Roy, R.: Short-term variability in halocarbons in relation to phytoplankton pigments in coastal waters of the central eastern Arabian Sea, Estuarine Coastal and Shelf Science, 88, 311-321, 10.1016/j.ecss.2010.04.011, 2010.

Saiz-Lopez, A., Fernandez, R. P., Li, Q., Cuevas, C. A., Fu, X., Kinnison, D. E., Tilmes, S., Mahajan, A. S., Gomez Martin, J. C., Iglesias-Suarez, F., Hossaini, R., Plane, J. M. C., Myhre, G., and Lamarque, J. F.: Natural short-lived halogens exert an indirect cooling effect on climate, Nature, 618, 967-973, 10.1038/s41586-023-06119-z, 2023.

Sala, S., Bönisch, H., Keber, T., Oram, D. E., Mills, G., and Engel, A.: Deriving an atmospheric budget of total organic bromine using airborne in situ measurements from the western Pacific area during SHIVA, Atmospheric Chemistry and Physics, 14, 6903-6923, 10.5194/acp-14-6903-2014, 2014.

Salawitch, R. J.: Atmospheric chemistry: biogenic bromine, Nature, 439, 275-277, 10.1038/439275a, 2006.

Sinnhuber, B. M., Sheode, N., Sinnhuber, M., Chipperfield, M. P., and Feng, W.: The contribution of anthropogenic bromine emissions to past stratospheric ozone trends: a modelling study, Atmospheric Chemistry and Physics, 9, 2863-2871, DOI 10.5194/acp-9-2863-2009, 2009.

Stemmler, I., Hense, I., and Quack, B.: Marine sources of bromoform in the global open ocean - global patterns and emissions, Biogeosciences, 12, 1967-1981, 10.5194/bg-12-1967-2015, 2015.

Tegtmeier, S., Atlas, E., Quack, B., Ziska, F., and Krüger, K.: Variability and past long-term changes of brominated very short-lived substances at the tropical tropopause, Atmospheric Chemistry and Physics, 20, 7103-7123, 10.5194/acp-20-7103-2020, 2020.

Tjiputra, J. F., Assmann, K., Bentsen, M., Bethke, I., Otterå, O. H., Sturm, C., and Heinze, C.: Bergen Earth system model (BCM-C): model description and regional climate-carbon cycle feedbacks assessment, Geoscientific Model Development, 3, 123-141, DOI 10.5194/gmd-3-123-2010, 2010.

Tjiputra, J. F., Schwinger, J., Bentsen, M., Morée, A. L., Gao, S., Bethke, I., Heinze, C., Goris, N., Gupta, A., He, Y. C., Olivié, D., Seland, O., and Schulz, M.: Ocean biogeochemistry in the Norwegian Earth System Model version 2 (NorESM2), Geoscientific Model Development, 13, 2393-2431, 10.5194/gmd-13-2393-2020, 2020.

Tokarczyk, R. and Moore, R. M.: Production of Volatile Organohalogens by Phytoplankton Cultures, Geophysical Research Letters, 21, 285-288, Doi 10.1029/94gl00009, 1994.

Villamayor, J., Iglesias-Suarez, F., Cuevas, C. A., Fernandez, R. P., Li, Q. Y., Abalos, M., Hossaini, R., Chipperfield, M. P., Kinnison, D. E., Tilmes, S., Lamarque, J. F., and Saiz-Lopez, A.: Very short-lived halogens amplify ozone depletion trends in the tropical lower stratosphere, Nature Climate Change, 13, 554-+, 10.1038/s41558-023-01671-y, 2023.

Wang, S. Y., Kinnison, D., Montzka, S. A., Apel, E. C., Hornbrook, R. S., Hills, A. J., Blake, D. R., Barletta, B., Meinardi, S., Sweeney, C., Moore, F., Long, M., Saiz-Lopez, A., Fernandez, R. P., Tilmes, S., Emmons, L. K., and Lamarque, J. F.: Ocean Biogeochemistry Control on the Marine Emissions of Brominated Very Short-Lived Ozone-Depleting Substances: A Machine-Learning Approach, Journal of Geophysical Research-Atmospheres, 124, 12319-12339, 10.1029/2019jd031288, 2019.

Wanninkhof, R.: The Impact of Different Gas Exchange Formulations and Wind Speed Products on Global Air-Sea CO2 Fluxes, in: Transport at the Air-Sea Interface, edited by: Garbe, C. S., Handler, R. A., and Jähne, B., Environmental Science and Engineering, Springer Berlin Heidelberg, Berlin, Heidelberg, 1-23, 10.1007/978-3-540-36906-6_1, 2007.

Warwick, N. J., Pyle, J. A., Carver, G. D., Yang, X., Savage, N. H., O'Connor, F. M., and Cox, R. A.: Global modeling of biogenic bromocarbons, Journal of Geophysical Research-Atmospheres, 111, Artn D24305 10.1029/2006jd007264, 2006.

Washington, J. W.: Hydrolysis Rates of Dissolved Volatile Organic-Compounds - Principles, Temperature Effects and Literature-Review, Ground Water, 33, 415-424, DOI 10.1111/j.1745-6584.1995.tb00298.x, 1995.

Yang, M. X., Bell, T. G., Bidlot, J. R., Blomquist, B. W., Butterworth, B. J., Dong, Y. X., Fairall, C. W., Landwehr, S., Marandino, C. A., Miller, S. D., Saltzman, E. S., and Zavarsky, A.: Global Synthesis of Air-Sea CO Transfer Velocity Estimates From Ship-Based Eddy Covariance Measurements, Front. Mar. Sci., 9, ARTN 826421 10.3389/fmars.2022.826421, 2022.

Ziska, F., Quack, B., Abrahamsson, K., Archer, S. D., Atlas, E., Bell, T., Butler, J. H., Carpenter, L. J., Jones, C. E., Harris, N. R. P., Hepach, H., Heumann, K. G., Hughes, C., Kuss, J., Krüger, K., Liss, P., Moore, R. M., Orlikowska, A., Raimund, S., Reeves, C. E., Reifenhäuser, W., Robinson, A. D., Schall, C., Tanhua, T., Tegtmeier, S., Turner, S., Wang, L., Wallace, D., Williams, J., Yamamoto, H., Yvon-Lewis, S., and Yokouchi, Y.: Global sea-to-air flux climatology for bromoform, dibromomethane and methyl iodide, Atmospheric Chemistry and Physics, 13, 8915-8934, 10.5194/acp-13-8915-2013, 2013.